Measurement 201 (2022) 111693

Contents lists available at ScienceDirect

Measurement

journal homepage: www.elsevier.com/locate/measurement

Heat flow measurement of human skin using a calorimetric sensor with a programmable thermostat. An alternative to climate chambers

Pedro Jesús Rodríguez de Rivera [a], Miriam Rodríguez de Rivera [b], Fabiola Socorro [a], Manuel Rodríguez de Rivera [a,*]

[a] Department of Physics, University of Las Palmas de Gran Canaria, Las Palmas de Gran Canaria, Spain
[b] Cardiology Service, University Hospital Marqués de Valdecilla, Santander, Spain

ARTICLE INFO

Keywords:
Direct calorimetry
Medical calorimetry
Skin heat loss
Skin heat flux, skin heat flow

ABSTRACT

In this paper we discuss the advantages of using a calorimetric sensor with a programmable thermostat compared to using heat flux sensors without a thermostat. The aim of this new calorimetric sensor is to measure the heat loss of the skin accurately. The sensor's measurement procedures and their experimental validation are shown. We also discuss the characteristics of the heat transfer phenomenon that takes place when a contact sensor is applied to the skin, emphasizing on the difficulties and opportunities that this type of measurement involves. This new thermostated calorimetric sensor is able to reproduce different temperature conditions on a localized skin region, providing a potential alternative to climate chambers. In addition, determining the heat flux for different thermostat temperatures allows the determination of an equivalent thermal conductance of the skin, that is directly related to its actual physiology. Finally, skin heat power is evaluated on different subjects and skin areas, and the results provided by our thermostated calorimetric sensor are compared with those provided by non-thermostated sensors.

1. Introduction

Human body's thermoregulation is a fascinating and complex mechanism. Under normal conditions, the organism is able to maintain a stable internal temperature of 36.7 to 37.5 °C [1]. For a subject at rest, values outside this range indicate that something abnormal is going on. The use of temperature as an indicator is a common denominator in many medicine specialties. Thermoregulation is composed of several mechanisms that simultaneously regulate the heat loss of the human body, such as breathing, sweating, vasoconstriction, vasodilation, etc. [2]. Heat loss through the skin is one of the mechanisms that contribute to the human body's thermoregulation. A typical human dissipates approximately 80 W at rest, but this value can increase up to 1400 W depending on the activity carried out [3]. Of this amounts, most of the heat is lost by evaporation, radiation and convection [4].

In the 18th century, Lavoisier and Laplace used an ice calorimeter to evaluate the heat loss of guinea pigs. This concept evolved into what we know today as direct calorimetry, which consists of confined spaces in which heat exchange is measured [5,6]. Also, indirect calorimetry was developed. This technique consists of relating the subject's energy output with its generated carbon dioxide volume (VCO_2) or consumed oxygen volume (VO_2), by means of empirical expressions. Both techniques - direct and indirect calorimetry - have been developed simultaneously, cross-validating mutually [7,8]. Nowadays, indirect calorimetry is the main technique used to express the energy cost of physical activities [9,10]. This energy is expressed in multiples of the resting metabolic rate (RMR), being the metabolic equivalent (MET) the unit used (1 MET corresponds to the consumption of 3.5 ml $kg^{-1}min^{-1}$ of O_2).

It is also relevant the measurement of heat loss from specific areas of the human body. Several authors performed localized heat flow measurements, in order to study heat loss at rest [11], as a function of clothing level [12], in response to heating and cooling events [13,14], exercise [15,16], or extreme climatic conditions [17]. Localized heat flux has also been measured to calculate the thermal resistance of the skin [17,18,19]. In this work, we focus on the localized heat flux measurements by means of contact sensors. Typically, heat flux sensors are essentially thermopiles. In contrast with the methods that obtain global measurements, localized measurement entails a particular difficulty. Heat flux sensors provide a direct and simple measurement, but the

* Corresponding author.
E-mail address: manuel.rguezderivera@ulpgc.es (M. Rodríguez de Rivera).

https://doi.org/10.1016/j.measurement.2022.111693
Received 20 March 2022; Received in revised form 18 July 2022; Accepted 27 July 2022
Available online 30 July 2022

sensor itself disturbs the heat flux in the measurement area. This leads to results that depend on this disturbance [20], different for each sensor and difficult to characterize. In addition, there is almost no standardization for measurements in living tissue. One efficient way to reduce the disturbance produced by the sensor is to make them minimally invasive, such as thin film heat flux sensors. On the other hand, the measurement of heat flow is the basis for the in-vivo measurement of the thermal properties of the skin (heat capacity, thermal conductivity). Therefore, it is of great interest to find a way to compare the results provided by different sensors [21].

In this paper, we present a calorimetric sensor based on a thermopile placed between the skin and a programmable thermostat, able to measure the heat flux, the heat capacity and the thermal resistance of the skin. In this work we focus on heat flow. The measurement of the thermal properties of the skin is addressed in parallel work [22,23,24]. In this work, we show the ability of the calorimetric sensor to estimate heat flux for different environmental conditions in a localized manner using a single instrument, which can be a useful complement to the use of climatic chambers. We describe the measurement procedures on the skin and validate them using a calibration base. Then, the characteristics of the heat transfer phenomenon that takes place when a contact sensor is applied to the skin are discussed. Next, we propose a method to compare the heat flux results determined with different contact sensors. Finally, skin heat power results in different areas of the human body in several subjects and under different thermal conditions are compared with other authors' data.

2. Materials and methods

2.1. Experimental system

The calorimetric sensor consists of a 13.2 × 13.2 × 2.2 mm^3 measurement thermopile (HOT20-65-F2A by Laird, part *a* in Fig. 1). Between this measurement thermopile and the skin, a 20 × 20 × 1 mm^3 aluminum plate is placed (part *b* in Fig. 1). A 14 × 14 × 4 mm^3 aluminum thermostat is located on the cold side of the thermopile, which contains a PT100 and a constantan heating resistor (part *c* in Fig. 1). The thermostat temperature is regulated by a proportional-integral-derivative controller (PID controller). Thermostat cooling is performed by a Peltier element (HOT20-65-F2A by Laird, part *d* in Fig. 1), a fan and a heatsink (part *e* in Fig. 1). The cooling system allows to control the thermostat temperature up to 10 °C under the ambient temperature [25]. Thermal insulation surrounds the lateral faces of the sensor, minimizing heat transfer by conduction, radiation and convection.

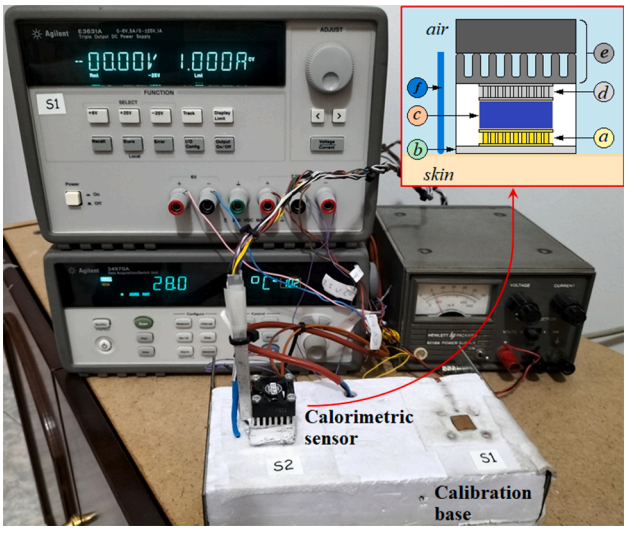

Fig. 1. Sensor in its calibration base and instrumentation used. Sensor schematic: (*a*) measuring thermopile, (*b*) aluminum plate, (*c*) thermostat, (*d*) Peltier element, (*e*) heat sink and fan, (*f*) thermistor.

The sensor's temperature operating range depends on the room temperature and the heating and cooling capacity of the sensor itself. In the prototype constructed, the sensor thermostat can be programmed between 22 and 40 °C for room temperatures between 18 and 28 °C. This calculation takes into account the maximum skin power for each temperature of the thermostat. We consider a heat flux of 0.1 Wcm^{-2} when the thermostat is at 28 °C.

Recently, a thermistor has been integrated on the side of the sensor to measure the skin temperature in the vicinity of the sensor (part *f* in Fig. 1). Fig. 1 displays a picture of the sensor in its calibration base and the instrumentation used. A schematic of the sensor is also shown. The calibration base consists of an insulating material that has two holders, where the sensor can be placed with a magnetic clamp. Each holder consists of a copper plate that contains an electrical resistance and a temperature sensor. A PID controller allows to control the temperature of the holder above the ambient temperature. Thus, the power and the temperature of the receptacle can be controlled. With this base, sensor calibration is performed under different temperature conditions of the base and the sensor thermostat.

We use a triple power supply (E3631A by Agilent) to power the resistors of the calibration base, the thermostat, and the Peltier element. A data acquisition system (34970A with 34901A by Agilent) reads the temperatures and the calorimetric signal. These instruments connected via GPIB bus (82357B by Agilent) to a laptop. An additional power supply (HP6216A) powers the sensor fan. The acquisition and control program has a sampling period of 0.5 s and is written in Microsoft Visual C++.

2.2. Calorimetric model and sensor's calibration

To relate the heat flux transmitted by conduction between the human skin and the sensor's thermostat, we need a model capable of accurately representing the operation of the sensor. For this purpose we use an RC modelling, very common in calorimetry [26,27,28]. In our model, we decompose the system into two elements of heat capacities C_1 and C_2 connected to each other by the measurement thermopile. The first element (C_1) represents a domain that includes the location of the heat power source W_1, the aluminum plate and the external surface of the measurement thermopile. The measured power W_1 is that of the skin where the sensor is placed, or the power of the calibration base. The second element (C_2) represents a domain that includes the sensor's thermostat and the reference surface of the measurement thermopile. These two elements – C_1 and C_2 – are connected to each other and to the outside by couplings of thermal conductances P_1, P_2 and P_{12}. These conductances characterize the steady-state heat transfer between the two domains (P_{12}) and between the domains and the environment, through the thermal insulation (P_2) and the calibration base itself (P_1). The conduction heat transfer equations define this model:

$$\begin{aligned} W_1(t) &= C_1\frac{dT_1}{dt} + P_{12}(T_1 - T_2) + P_1(T_1 - T_{room}) \\ W_2(t) &= C_2\frac{dT_2}{dt} + P_{12}(T_2 - T_1) + P_2(T_2 - T_{cold}) \\ y(t) &= k(T_1 - T_2) \end{aligned} \quad (1)$$

In Eq. (1), W_1 and W_2 are the powers of each element. The measuring thermopile provides the calorimetric signal *y* (t), which is proportional to the temperature difference between the thermopile surfaces (T_1 and T_2). The ambient temperature is T_{room}, and the cold focus of the thermostat, controlled by the Peltier element, is at T_{cold}.

The calibration base has two purposes. First, the base is used to perform experimental simulations in order to calibrate the sensor and study its performance under different power and temperature settings.

Our aim is to replicate the skin's behavior. The second function of the calibration base is to provide an initial steady state, in which the time derivative of all temperatures and powers are zero. When this steady state is reached, the baselines are corrected. Operating the system Eq. (1), we obtain the system Eq. (2), where ΔT_0 is the variation of the temperature that surrounds the sensor, when the sensor is moved from the base to the human skin [29].

$$\begin{aligned}\Delta W_1 &= \frac{C_1}{k}\frac{d\Delta y}{dt} + \frac{P_1+P_{12}}{k}\Delta y + C_1\frac{d\Delta T_2}{dt} + P_1(\Delta T_2 - \Delta T_0)\\ \Delta W_2 &= -\frac{P_{12}}{k}\Delta y + C_2\frac{d\Delta T_2}{dt} + P_2(\Delta T_2 - \Delta T_0)\end{aligned} \tag{2}$$

The sensor is calibrated using a specific experimental measurement designed for this purpose. With the sensor placed in the calibration base, a sequence of different temperatures of the calibration base and sensor thermostat is programmed. The base and thermostat temperature controls determine the powers to maintain the programmed temperatures, and the measurement thermopile provides the calorimetric signal. Fig. 2 shows a calibration measurement. The curves mentioned above are represented in it. In this case the temperature of the calibration base is programmed from 32 to 34 °C and the thermostat temperature from 28 to 30 °C, the ambient temperature being 20.5 °C. Knowing these experimental curves, the parameters of the model relating these variables are determined (Eq. (2)). In a recent work a detailed study on the calibration of this sensor was performed [24]. The model parameters C_1, C_2, P_1, P_2, P_{12} and k are given in Table 1. The Joule calibrations allow us to determine the resolution of the sensor, obtaining a value of 1 mW/cm^2 for the heat flux. In these calibrations, the difference between the measured heat flux and the base calibration 'power is up to 3%. In the human skin, the uncertainty will depend mainly on the temperature of the thermostat, the zone, and the physical state of the subject [23]. For example, for the sensor thermostat at 24 °C, the measured heat flux is of the order of 60 mWcm^{-2}, which is equivalent to an uncertainty of 2%. If the measurement is performed with the thermostat at 32 °C, the measured heat flux is of the order of 20 mWcm^{-2}, and the uncertainty rises to 5%. However, if the thermostat is set at 36 °C, the heat flux will be of the order of 4 mWcm^{-2}, which is equivalent to an uncertainty of 25%.

Table 1
Calorimetric Model parameters (Eq. (1) and (2)).

Parameter		Unit	Parameter		Unit
C_1	2.780	JK^{-1}	P_1	0.029	WK^{-1}
C_2	4.730	JK^{-1}	P_2	0.055	WK^{-1}
P_{12}	0.125	WK^{-1}	k	22.70	mVK^{-1}

2.3. Measurement procedure

The programmable thermostat contained in the calorimetric sensor allows to design multiple measurement procedures. In this paper we present the two main procedures.

a. Measurements at constant thermostat temperature.

Before applying the sensor on the skin, the sensor is placed on the calibration base. An initial temperature of the sensor's thermostat is programmed, and when steady state is reached in the calibration base, the sensor is applied on the skin until steady state is reached again on the skin. Finally, the sensor is placed back on the calibration base. This procedure can be repeated for different constant thermostat temperatures. For each measurement, the sensor is applied on the skin for 5 min.

b. Measurements with linear variation of the thermostat temperature.

This procedure is a continuation of the previous case. While the sensor is on the skin, and when steady state is reached at the initial set thermostat temperature, a second thermostat temperature is programmed. The transition between the two thermostat temperatures is linear, and the measurement continues until the steady state – on the skin – is reached. This procedure provides two heat power values at two different thermostat temperatures in a single measurement. The sensor is applied on the skin for 12 min.

These procedures have been validated with experimental measurements using the calibration base. For this purpose, the sensor is placed on the first holder of the calibration base, where $W_1 = 0$. When steady state is reached for an initial set thermostat temperature, the sensor is

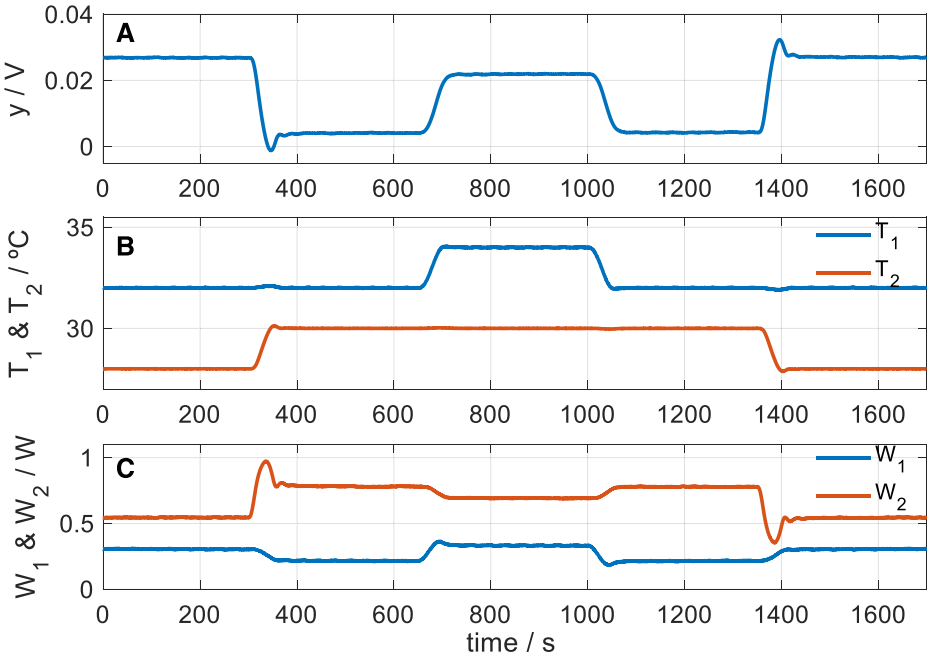

Fig. 2. Experimental calibration measurement. (A) Calorimetric signal y. (B) Temperatures of calibration base T_1 (red) and thermostat T_2 (blue). C) Powers of calibration base W_1 (red) and thermostat W_2 (blue). Room temperature $T_{room} = 20.5$ °C. (For interpretation of the references to colour in this figure legend, the reader is referred to the web version of this article.)

placed on the second holder, where a heat power is applied to maintain the holder at a constant temperature. The aim of these measurements is to replicate the behavior of the sensor when it is placed on the skin.

Fig. 3 shows the experimental curves of a measurement with linear variation of the thermostat temperature T_2, performed on the calibration base. The programming of this measurement is the same as that used when the sensor is applied to the skin. Initially, the sensor is placed in *holder 1* of the calibration base (see Fig. 1) where there is no heat power, and the sensor's thermostat is set at a temperature $T_2 = 28$ °C. When steady state is reached (instant t_1 in Fig. 3), the sensor is placed in *holder 2*, whose temperature is constant ($T_{base} = 35$ °C). When steady state is reached in *holder 2*, the temperature of the sensor thermostat is linearly increased to a temperature of $T_2 = 33$ °C at a rate of 3 Kmin^{-1} (from instant t_2 to t_3). This temperature $T_2 = 33$ °C is maintained until the new steady state is reached in *holder 2*. Fig. 3 shows the calorimetric signal (y) and the temperatures of the base (T_{base}) and the sensor's thermostat (T_2). The power of the calibration base (W_1) to maintain the temperature $T_{base} = 35$ °C, and the power of the sensor thermostat (W_2) to control the temperature T_2 are also shown.

The method used to calculate the power W_1 that passes through the sensor is explained in detail in previous works [25,29]. The procedure consists of an iterative process based on the Nelder-Mead method [30]. An algorithm that minimizes the error between the experimental and the calculated curves of the calorimetric signal and the thermostat temperature is used. A power function with a predefined shape is proposed for this purpose, according to the temperature programmed in the measurement. In the case of Fig. 1, the power is represented by Eq. (3):

$$\begin{aligned} W_1(t) &= 0 && for\ t < t_1 \\ W_1(t) &= A_0 + A_1 \exp\left(-\frac{t-t_1}{\tau_1}\right) && for\ t_1 \leqslant t \leqslant t_2 \\ W_1(t) &= W_1(t_2) + \Delta A_0 \frac{t-t_2}{t_3-t_2} && for\ t_2 \leqslant t \leqslant t_3 \\ W_1(t) &= W_1(t_2) + \Delta A_0 && for\ t \geqslant t_3 \end{aligned} \tag{3}$$

Being t_1 the instant in which the sensor is placed on the heat source, and t_2, t_3 the instants that limit the time interval in which the thermostat temperature is linearly increased. Thus, the power W_1 is defined by the parameters A_0, ΔA_0, A_1 and τ_1. The exponential of amplitude A_1 represents the transient due to the placement of the sensor on the heat source. With these parameters, the power W_1 is reconstructed. Knowing the two powers – W_1 and W_2 – the calorimetric signal and the thermostat temperature T_2 are reconstructed using the calorimetric model (Eq. (2) and Table 1). Fig. 4 shows the calculated power W_1 and the fittings of the calorimetric signal and the thermostat temperature. Note the good fitting of the calculated W_1 power, either for the stationary zones and for the transient zone produced by the placement of the sensor on the heat source. The error in the calculation of the power W_1 is about 4%. For the case represented, $A_0 = 349$ mW, $\Delta A_0 = -216$ mW, $A_1 = 245$ mW and $\tau_1 = 7$ s.

The chosen temperature increase of 5 °C is adequate to determine the heat power output with enough accuracy. Increasing the temperature step increases the signal-to-noise ratio. However, in our sensor, a thermostat temperature increase of more than 10 °C can saturate the sensor. The sensor is saturated when the programmed temperature is not reached.

The described deconvolution process allows the heat flux to be determined even if the steady state of the calorimetric signal has not been reached. However, there is a limit directly related with the

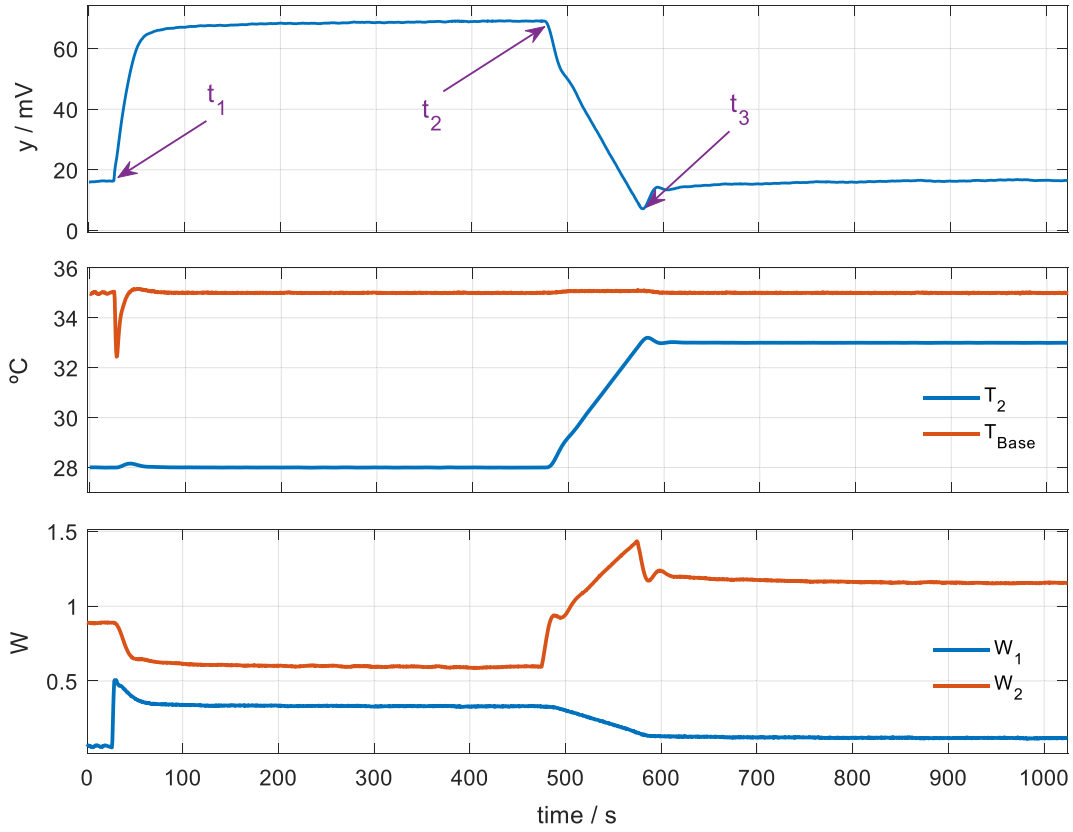

Fig. 3. Experimental curves of a verification measurement of the sensor performance. Calorimetric signal (y). Temperatures of the calibration base (T_{base}) and thermostat (T_2). Calibration base (W_1) and thermostat (W_2) powers.

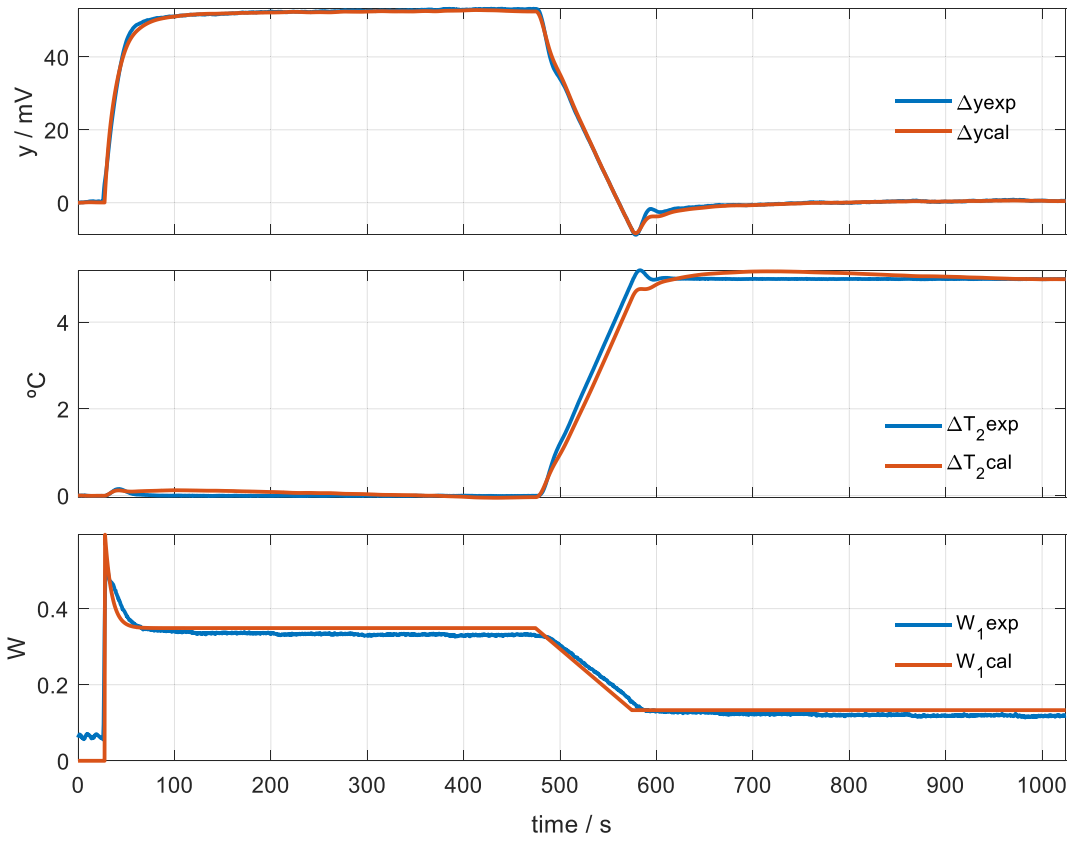

Fig. 4. Experimental verification measurement of the sensor performance in the calibration base. Experimental and model-calculated curve fits. Calorimetric signal (Δy), thermostat temperature (ΔT_2) and power W_1.

sensitivities and time constants of the system. It is necessary at least 300 s from the end of the linear temperature variation of the thermostat.

2.4. Measurement on human skin

In this section, the measurement methods described previously are applied in the human body.

c. Measurements at constant thermostat temperature.

Fig. 5 shows the calculated heat flux of four measurements made on the sternum of a healthy 63-year-old male subject seated and at rest, at an ambient temperature of 24.4 °C. These measurements were performed at different sensor's thermostat temperatures $T_2 = 24$, 28, 32 and 36 °C. The initial power peaks, consequence of the placement of the sensor on the skin, are marked. This initial power peak increases as the thermostat temperature decreases. This means a higher difference between the skin and sensor temperatures. Note that the heat flux W_1 depends on the sensor's thermostat temperature. Several authors remark that there is a dependence between skin heat loss and environmental conditions [16,17]. As the difference between the skin temperature T_{skin} and the ambient temperature T_{room} is larger, heat flux increases. In our case, the reference temperature is not T_{room}, it is the sensor's thermostat temperature, T_2. On the other hand, these results should be understood as the response to the perturbation of placing a cold surface of high thermal conductivity (the sensor) on the skin. In this configuration, the heat flux is magnified over the natural value. In this paper we will emphasize on this relationship.

d. Measurements with linear variation of the thermostat temperature.

In the second case, we show a measurement in the volar area of the left wrist of a healthy 63-year-old male subject seated and at rest. The ambient temperature was 25.1 °C.

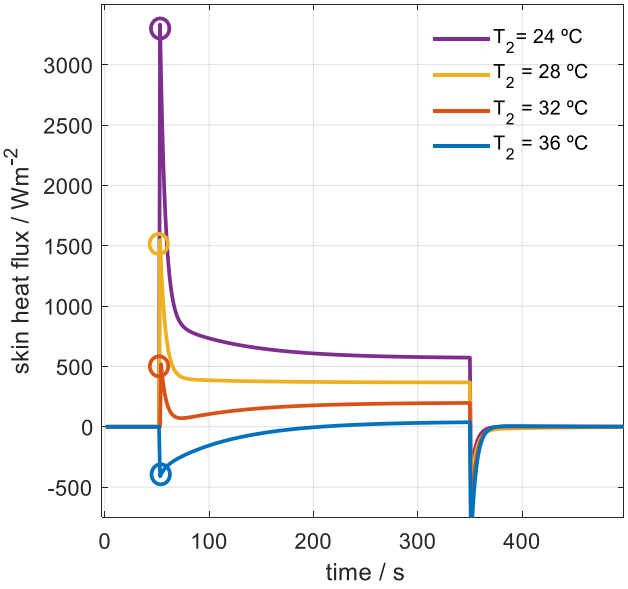

Fig. 5. Heat flux measured in the sternum of a healthy 63-year-old male subject at rest for different sensor's thermostat temperatures $T_2 = 24$, 28, 32 and 36 °C ($T_{room} = 24.4$ °C). The circles indicate the amplitude of the initial transient power for each measurement.

Initially, the sensor is placed on the calibration base and the thermostat is programmed at a constant temperature $T_2 = 28$ °C. When steady state is reached, the sensor is applied on the skin (Fig. 6) until

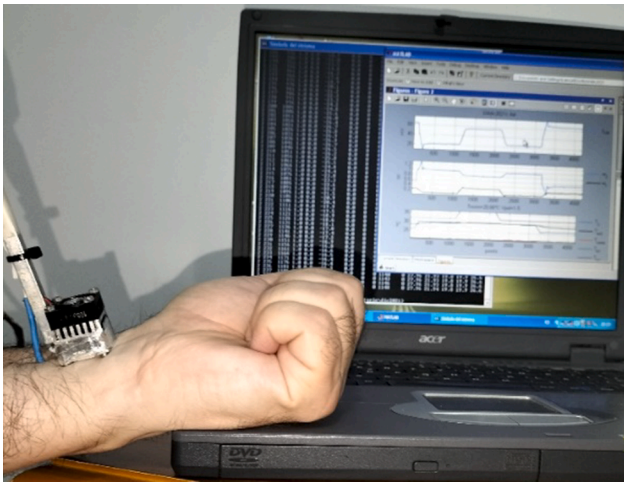

Fig. 6. Application of the sensor on the volar area of the left wrist of a healthy 63-year-old male subject at rest.

steady state is reached. The thermostat temperature is then linearly increased to $T_2 = 33$ °C at a rate of 3 Kmin^{-1}. This temperature is maintained until the end of the measurement. Fig. 7 shows the calculated heat flux and the fittings of the calorimetric signal and thermostat temperature. The parameters that define the power function are $A_0 = 176$ mW, $\Delta A_0 = -137$ mW, $A_1 = 1350$ mW and $\tau_1 = 5$ s (see Eq. (3)).

Linear temperature programming has the advantage of allowing the new temperature to be progressively reached. At the end of the linear temperature variation, there is a calorimetric signal transient (see red arrow in Fig. 7) which is directly related with the heat capacity of the skin and allows to determine it [23].

In Fig. 7 the function ΔT_0 has also been represented (see Eq. (2)). This function represents the increase of the temperature that surrounds the sensor when the location is changed: from the calibration base to the skin. Considering an exponential increase, we obtain as a result an amplitude of 1.56 °C and a time constant of 84 s.

2.5. Normalization and interpretation of measurements

When skin heat flux is measured with contact sensors, there may be substantial differences in the results depending on the instrument used. In this section, three aspects will be discussed: (1) the relationship between the signal provided by the sensor (usually a measurement thermopile) and the heat flux, (2) the effect of the contact between the sensor and the skin on the cutaneous heat flux, and (3) a proposed standardization of the results obtained by different heat flux sensors.

2.5.1. Relationship between the signal provided by the thermopile and the heat flux

Many authors who use thermopiles as heat flux sensors consider the heat flux proportional to the signal provided by the thermopile [12,13,15,11,17,31], and the calibrations are usually performed with stepped stationary heat powers [12,16]. This consideration implies that the reference surface of the thermopile is at a constant ambient temperature. This assumption is an inaccurate approximation: the heat flow through the thermopile will change the reference temperature, which won't be the ambient temperature anymore. As consequence, the reference is not properly defined. For this reason, in many works, more importance is given to relative values [32,13,33,34] than to absolute values, taking the initial state of heat power as a reference. On the other hand, few authors consider transient states in the measurement of heat flow [14]. When the sensor is placed on the skin or when the skin heat loss changes, part of the heat loss of the human body is invested in varying its own temperature and the temperature of the measuring instrument. In order to quantify this energy and, therefore, to obtain an

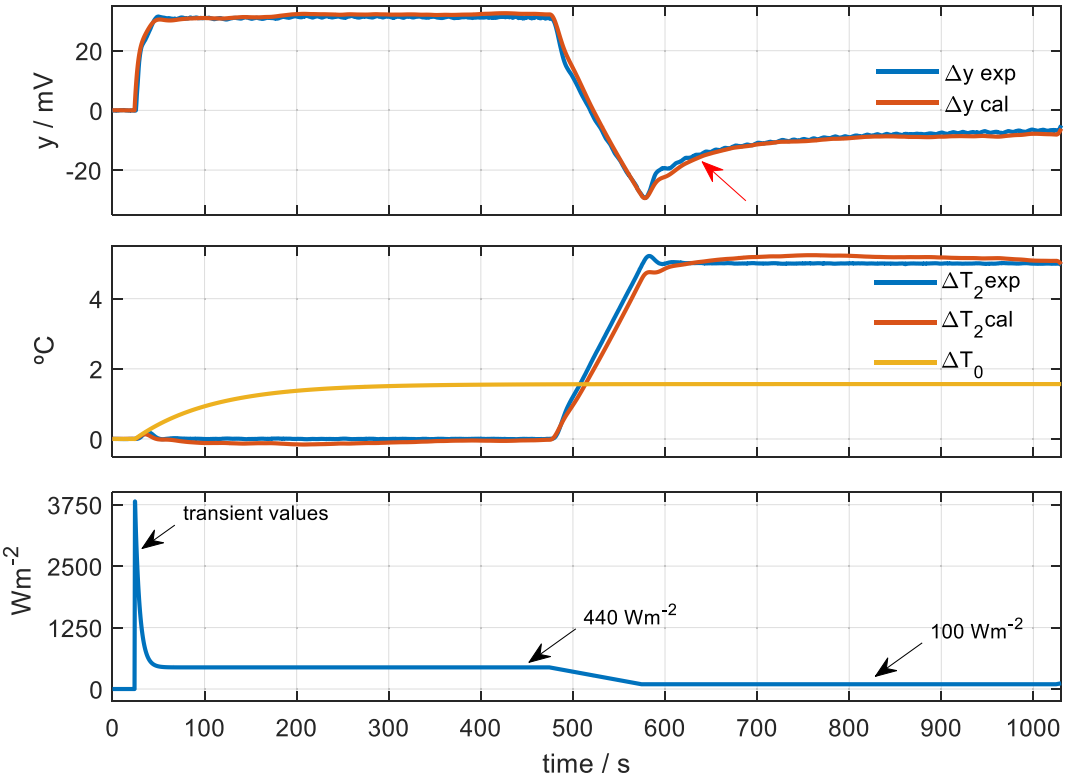

Fig. 7. Measurement in the volar area of the left wrist in a healthy 63-year-old male subject, at rest. Fitting of the calorimetric signal (Δy). Fitting of the thermostat temperature (ΔT_2) and variation of the temperature that surrounds the sensor (ΔT_0). Heat flux measured by the sensor. Initial thermostat temperature $T_2 = 28$ °C ($T_{room} = 25.1$ °C).

accurate balance of the energy transferred by the human body during the transient state, it is necessary to consider the heat capacities of the bodies involved in the heat transfer phenomenon. An alternative way to obtain an accurate balance consists of using instruments that have a very low thermal inertia [34]. In previous works we have shown the interest of performing measurements while varying the temperature of the sensor thermostat, and studying the corresponding transient states [29,23]. In our sensor, the novelty is that the reference of the measurement thermopile is the controlled temperature of the thermostat, T_2. The relationship between the powers, the calorimetric signal and the reference temperature (thermostat) is well represented by Eq. (2).

2.5.2. Effect of the sensor on cutaneous heat flow

Heat flux sensors provide a simple and direct measurement, but the sensor itself disturbs the heat loss of the studied region, leading to results conditioned to this disturbance. Fig. 8 illustrates this problem. In a natural case, in which the skin is naked, the human body emits a heat power W_N (natural). This heat power is proportional to an overall heat transfer coefficient – or natural equivalent thermal conductance – P_N (WK^{-1}) between two thermal sources: the skin and the environment, defined by the temperatures T_{skin} and T_{room}. However, when a sensor is placed on the skin, the device itself can act as a thermal insulator, resulting in a decrease of the equivalent thermal conductance ($P < P_N$). This causes a lower heat flux ($W < W_N$) [20]. The opposite can also happen. A sensor with certain thermal properties could facilitate heat transfer ($P > P_N$). As a consequence, the heat flux would increase ($W > W_N$). The measured heat power W depends on the conductance between the skin and the environment through the sensor. This situation is problematic: the heat flux results depend on the characteristics of the instrument. This justifies that in works in which this magnitude is measured, direct heat flux data are often not provided. Instead, statistical results or relative values are provided, as mentioned above [32,13,33,34].

Our sensor has a thermostat inside. By controlling its temperature, the cold focus of the heat transfer phenomenon becomes inside the instrument itself. This is a great advantage, since heat transfer by radiation and convection is minimized, and the predominant mechanism is conduction. The thermal perturbation produced by our sensor consists of connecting the skin with a controllable cold source through a constant and known equivalent thermal conductance, of value P_{12} (see Table 1).

Table 2 shows the specifications of two types of sensors: foil heat flux sensors and plate heat flux sensors. Our sensor is of the second type, but with a built-in thermostat. Standard units are used in the table. The high sensitivity of our sensor, compared to others, is due to the thermostat located on the reference surface of the measuring thermopile. This configuration is typical for all commercial calorimeters. In commercial heat flux sensors this configuration is not used, and they are very sensitive to environmental disturbances and require controlled thermal environments. With our sensor it is not necessary to work in a controlled environment. However, the result obtained with our sensor is not a natural heat flow: it is the thermal response to the perturbation produced by the presence of the sensor on the skin. This type of measurement is appropriate to determine the thermal properties of the skin [35] that require the knowledge of this heat flux, a field that we addressed in other works. In this work we study the relationship between the heat flux measured with different sensors (see Fig. 8).

2.5.3. Comparison of heat flux results

How to compare heat flux measurements made with different sensors? In this section we propose a possible solution, which consists of calculating the natural heat power. Natural heat power is the heat power in the case where no sensor is applied. We consider two situations: a) skin heat power W_N in a natural situation between the skin (T_{skin}) and the ambient (T_{room}) and b) heat power W through the sensor, in the same area, between the skin and the temperature of the thermopile's cold side (T_{ref}).

$$\begin{aligned} W_N &= P_N(T_{skin} - T_{room}) \\ W &= P(T_{skin} - T_{ref}) \end{aligned} \tag{4}$$

Operating, we obtain an expression that relates the natural heat flux (W_N) with that measured by the sensor (W):

$$W_N = \frac{P_N}{P} W + P_N(T_{ref} - T_{room}) \tag{5}$$

With Eq. (5), a natural heat power value can be estimated from the measured value (W) and the environmental conditions of the experiment. To calculate the natural heat power W_N we must know five quantities (P_N, P, W, T_{ref} and T_{room}). Let consider that the measured heat flux W and the ambient temperature T_{room} are both known. The overall heat transfer coefficient of the natural skin-air system (P_N) can be approximated by the expression of Kurazumi, Y. [37]. This empirical expression allows to evaluate this conductance as a function of humidity, air velocity and ambient temperature. It remains to know P and T_{ref}. These quantities are related with the measuring instrument itself. In a passive sensor where the reference is in the air, P and T_{ref} will depend on factors outside the sensor, such as air velocity. In our case the advantage is that P and T_{ref} are known: $T_{ref} = T_2$ and $P = P_{12}$. By applying Eq. (5), we can compare our results with those obtained by other authors using

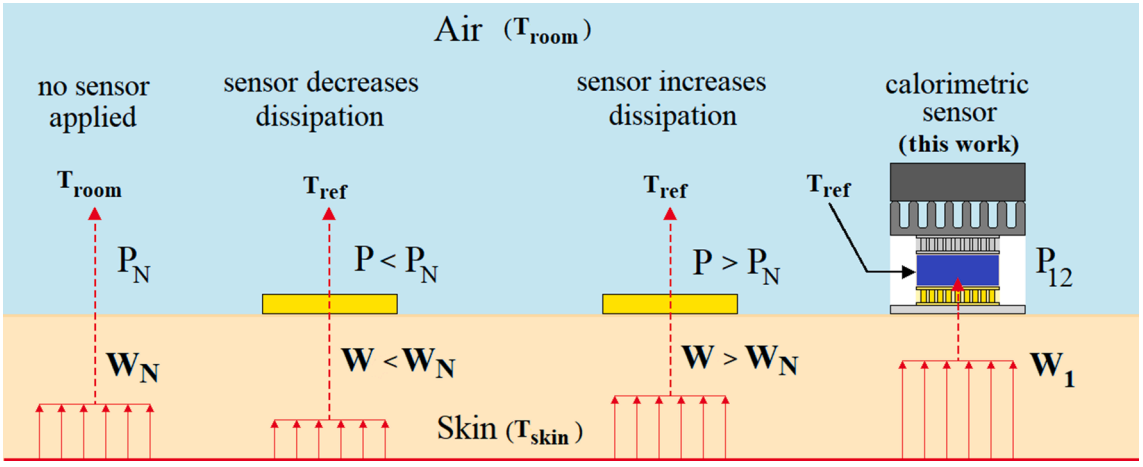

Fig. 8. Illustration of the magnitude of the human skin heat flux (W) in a natural case (W_N) and through different contact sensors. P represents the thermal conductance between the skin and the environment. In the case of the thermostated sensor (this work), heat flux W_1 is transmitted by conduction between the skin and the thermostat through a thermal conductance P_{12} (Eq. (2) and (3)).

Table 2
Specifications of different heat flux sensors.

Heat flux sensor	Sensitivity $\mu V/(Wm^{-2})$	mVW^{-1}	Sensing area cm^2	thickness mm	Thermal resistance $K/(Wm^{-2})$	K/W	Conductance $P\ (mWK^{-1})$
Foil heat flux FHF04 [36]	11	4.4	25.0	1.0	30×10^{-4}	1.20	833.3
Foil heat flux FHF03 [36]	2	8.0	2.5	1.0	28×10^{-4}	11.20	89.3
Heat flux plate HFP01 [36]	60	75.0	8.0	5.4	71×10^{-4}	8.88	112.6
Heat flux plate HFP03 [36]	500	78.1	64.0	5.4	71×10^{-4}	1.11	900.9
Calorimeter sensor (this work)	59	147.7	4.0	(*)	37×10^{-4}	8.0	125.0

(*) The measuring thermopile has an area of $13.2 \times 13.2\ mm^2$ and a thickness of 2.2 mm.

heat flux sensors without thermostat and whose reference is the ambient temperature ($T_{ref} = T_{room}$).

3. Results and discussion

Fig. 9 shows experimental values of heat flux (in Wm^{-2}) in different areas of the human body at rest, as a function of the reference temperature: the thermostat temperature ($T_{ref} = T_{room}$) in our sensor, and ambient temperature ($T_{ref} = T_{room}$) in the case of sensors without thermostat.

With our sensor, measurements have been performed in different environmental conditions, in seven different areas (temple, sternum, abdomen, hand, hand, wrist, thigh and heel) of 16 subjects (Table 3). Subjects were at rest and normally clothed. This study was conducted in accordance with the principles of the Declaration of Helsinki. All subjects received oral and written information about the purposes, risks and benefits of the study before giving written consent.

In Fig. 9 we present a summary of the measurements performed on

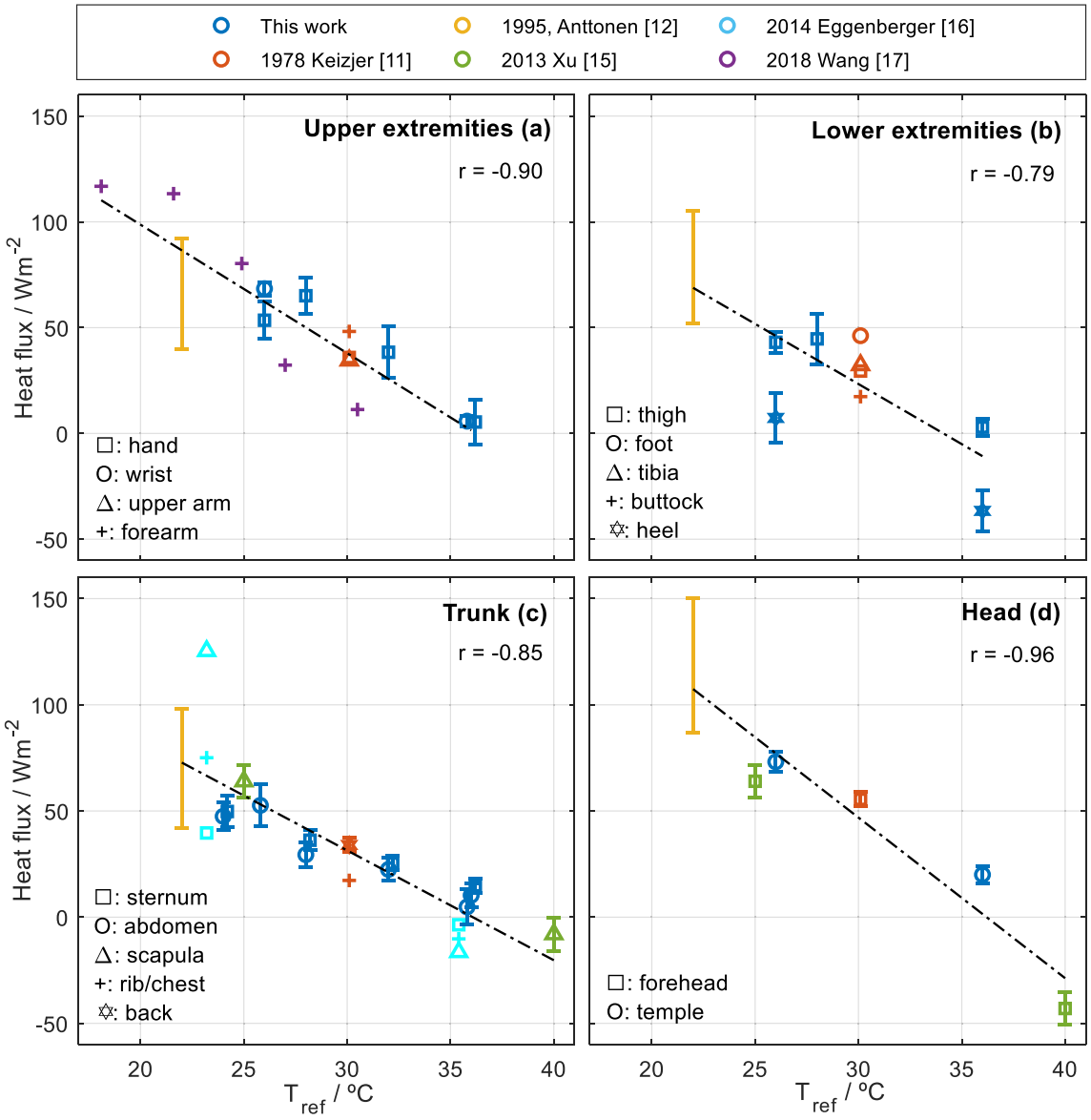

Fig. 9. Experimental heat flux measurements (in Wm^{-2}) for different subjects at rest in different areas of the human body, as a function of the reference temperature (T_{ref}). Overall, results are presented for 16 zones and 124 subjects, obtained by six research teams.

Table 3
Anthropometric characteristics of the subjects who participated in the studies with our sensor (M: male, F: female).

Subject	Age (years)	Mass (kg)	Height (cm)	Sex	Subject	Age (years)	Mass (kg)	Height (cm)	Sex
1	62	71.0	160	M	9	25	76.0	181	M
2	29	68.0	172	M	10	24	79.0	172	M
3	27	83.0	177	M	11	20	80.0	168	M
4	57	68.0	166	F	12	21	–	–	F
5	31	74.0	149	F	13	21	54.0	160	F
6	24	53.0	161	F	14	23	54.0	155	F
7	25	–	–	M	15	20	74.0	168	F
8	23	72.0	168	M	16	29	88.0	169	F

these subjects [23,38], having applied the normalization proposed in the previous section (Eq. (5)). This normalization uses the Kurazumi expression [35] and allows us to obtain an approximation of the natural heat flow in different areas as a function of the ambient or reference temperature. We have also considered measurements performed by other authors [11,12,15,16,17]. Fig. 9 shows average results in 16 areas and 124 subjects, obtained by six different research teams.

Heat flux is different for each human body area. Highest values are at the head, and smallest ones at the lower extremities, being especially low at the heel [11,12,15]. The trunk and upper extremities present an intermediate situation. In the same place and under the same environmental conditions, the resting heat flux can vary by 25% [38]. In this work we highlight the variation of cutaneous heat flux as a function of T_{ref}. The heat flux approaches zero as T_{ref} approaches T_{skin}, and if T_{ref} keeps decreasing, the heat power increases in magnitude, but in the opposite direction (negative sign). Table 4 shows the characteristics of the regression line represented in each of the graphs in Fig. 9.

As we can see, there is a significant correlation between the heat flux and T_{ref}. As expected, it is always negative and different in each region. The slope is directly related with the thermal conductance of the skin zone studied. The head zones present the highest conductance and the trunk zones the lowest. Note that several of the referenced works employ climatic chambers to achieve the desired environmental conditions in the experiment [11,15,16,17]. In our case, we obtain similar results for different environmental conditions by adequately programming the sensor's thermostat. Calorimetric sensors with programmable thermostat are a useful complement for studying the human physiology, since they allow the simulation of different environmental conditions in a localized way.

In this work we show results for different subjects at rest. With our sensor, measurements have also been made on subjects performing physical exercise on a cycle ergometer in a previous work [22]. In these cases, there is a 20 to 40% heat flow increase that depends on the subject. We have also detected different heat flow recovery depending on the subject.

We can say that the heat flow measured by the sensor is artificial, since it is the response to a perturbation that consists of placing the sensor on the skin and varying the temperature of the device. Instead of minimizing the possible perturbation that the sensor can produce on the skin, this instrument tries to apply a controllable and systematic perturbation, whose response is studied. This response measured by the sensor describes how a specific skin area behaves in vivo when the temperature changes. This allows the determination of skin heat capacity and thermal resistance, which are related with the degree of vasoconstriction or vasodilatation of the skin.

Table 4
Regression lines for human body zones.

	Pearson correlation	Regression line: $W = a + b\,T_{ref}$	
Zone	r	a/Wm^{-2}	$b/Wm^{-2}{}^{\circ}C^{-1}$
Upper extremities	−0.90	194	−5.68
Lower extremities	−0.79	220	−6.07
Trunk zones	−0.85	187	−5.17
Head zones	−0.96	274	−7.56

4. Conclusions

The determination of heat flow in localized areas of the human body is of great interest for the study of thermoregulation of the human body. Although heat flow sensors provide a simple measurement, the heat transfer phenomenon is altered by the instrument itself. In this paper, we present a calorimetric sensor with a programmable thermostat, which has several advantages over heat flow sensors without a thermostat:

- It allows to know and compensate the effects of the thermal disturbance produced by the sensor, obtaining a good approximation of the natural heat flow of the human body.
- The sensor is designed to measure heat flow by conduction from the skin to the sensor thermostat, and convection and radiation phenomena on the sensor are minimized. This is a different way of evaluating skin heat flow.
- The sensor allows the determination and monitoring of the thermal conductance of the measured skin area. This conductance is defined as the slope of the heat flow with respect to the reference temperature.
- This calorimetric sensor with programmable thermostat is therefore a useful instrument that could complement the study of human thermoregulation: by programming the sensor's thermostat appropriately, it is possible to simulate different ambient temperature conditions in a localized manner. We have contrasted our results with those of other authors that use climatic chambers, obtaining similar results. For this reason, this instrument could be an alternative to the use of climatic chambers.

CRediT authorship contribution statement

Pedro Jesús Rodríguez de Rivera: Investigation, Methodology, Writing – review & editing. **Miriam Rodríguez de Rivera:** Investigation, Supervision, Writing – review & editing. **Fabiola Socorro:** Conceptualization, Investigation, Methodology, Validation. **Manuel Rodríguez de Rivera:** Investigation, Supervision, Writing – review & editing.

Funding

This work research was funded by the "Consejería de Economía, Conocimiento y empleo del Gobierno de Canarias, Programa Juan Negrín" grant number SD-20/07 (grant holder: Pedro Jesús Rodríguez de Rivera).

Declaration of Competing Interest

The authors declare that they have no known competing financial interests or personal relationships that could have appeared to influence the work reported in this paper.

Data availability

Data will be made available on request.

References

[1] M. Sund-Levander, C. Forsberg, L.K. Wahren, Normal oral, rectal, tympanic and axillary body temperature in adult men and women: A systematic literature review, Scand. J. Caring Sci. 16 (2) (2002) 122–128, https://doi.org/10.1046/j.1471-6712.2002.00069.x.

[2] Y. Hoydas, E.F.J. Ring, Human Body Temperature: Its Measurement and Regulation, New York & London, 1982.

[3] M.N. Cramer, O. Jay, Biophysical aspects of human thermoregulation during heat stress, Autonomic Neurosci. 196 (2016) 3–13, https://doi.org/10.1016/j.autneu.2016.03.001.

[4] J.B. Cain, S.D. Livingstone, et al., Respiratory heat loss during work at various ambient temperatures, Respir. Physiol. 9 (2) (1997) 145–150, https://doi.org/10.1016/0034-5687(90)90014-P.

[5] J.W. Snellen, K.S. Chang, W. Smith, Technical description and performance characteristics of a human whole-body calorimeter, Med. Biol. Eng. Comput. 21 (1983) 9–20, https://doi.org/10.1007/BF02446401.

[6] J.W. Snellen, P. Baskind, The air-conditioning system, and operation and performance of the human calorimeter of the Human Sciences Laboratory. C.O.M. Report No. 24/69, Chamber of Mines of South-Africa, 1969.

[7] H. Mtaweh, L. Tuira, A.A. Floh, C.S. Parshuram, Indirect calorimetry: history, technology, and application, Front. Pediatrics 6 (2018) 257, https://doi.org/10.3389/fped.2018.00257.

[8] G.P. Kenny, S.R. Notley, D. Gagnon, Direct calorimetry: a brief historical review of its use in the study of human metabolism and thermoregulation, Eur. J. Appl. Physiol. 117 (2017) 1765–1785, https://doi.org/10.1007/s00421-017-3670-5.

[9] V.G. Fabiano Alves, E.E.M. da Rocha, M.C. Gonzalez, R.B. Vieira da Fonseca, M. H. do Nascimento Silva, Resting energy expenditure measured by indirect calorimetry in obese patients: variation within different BMI ranges, J. Parenter. Enter. Nutr 44 (1) (2020) 129–137, https://doi.org/10.1002/jpen.1589.

[10] J.R. Speakman, C. Selman, Physical activity and resting metabolic rate, Proc. Nutr. Soc. 62 (3) (2003) 621–634, https://doi.org/10.1079/PNS2003282.

[11] A. Keijzer, M. Woerlee, B.D. Kluver, M. Buist, Direct measurement of sensible heat transfer between man and his environment, J. Appl. Physiol. 33 (1972) 677–680, https://doi.org/10.1152/jappl.1972.33.5.677.

[12] H. Anttonen, K. Puhakka, J. Niskanen, P. Ryhänen, Cutaneous heat loss in children during anaesthesia, Br. J. Anaesthesia 74 (1995) 306–310, https://doi.org/10.1093/bja/74.3.306.

[13] J.R. House, M.J. Tipton, Using skin temperature gradients or heat flux measurements to determine thresholds of vasoconstriction and vasodilatation, Eur. J. Appl. Physiol. 88 (2002) 141–145, https://doi.org/10.1007/s00421-002-0692-3.

[14] Z. Ostrowski, Modelling and validation of transient heat transfer processes in human skin undergoing local cooling, Przegląd Elektrotechniczny 1 (2015) 78–81, https://doi.org/10.15199/48.2015.05.20.

[15] X. Xu, A.J. Karis, M.J. Buller, W.R. Santee, Relationship between core temperature, skin temperature, and heat flux during exercise in heat, Eur. J. Appl. Physiol. 113 (9) (2013) 2381–2389, https://doi.org/10.1007/s00421-013-2674-z.

[16] P. Eggenberger, et al., Prediction of core body temperature based on skin temperature, heat flux, and heart rate under different exercise and clothing conditions in the heat, Front. Physiol. 9 (2018) 1780, https://doi.org/10.3389/fphys.2018.01780.

[17] L. Wang, D. Chong, Y. Di, H. Yi, A revised method to predict skin's thermal resistance, Therm. Sci. 22 (2018) 1795–1802, https://doi.org/10.2298/TSCI1804795W.

[18] R.J. Osczevski, Thermal Resistance of the Cheek in Cold Air, Report No: 94-47, Defence and Civil In-stitute of Environmental Medicine, Toronto, Canada, 1994.

[19] D. Brajkovic, M.B. Ducharme, Cheek Skin Temperature and Thermal Resistance in Active and Inactive Individuals during Exposure to Cold Wind, J. Ther. Biol. 29 (7–8) (2004) 831–837, https://doi.org/10.1016/j.jtherbio.2004.08.068.

[20] J. Frim, M.B. Ducharme, Heat flux transducer measurement error: a simplified view, J. Appl. Physiol. 74 (4) (1993) 2040–2044, https://doi.org/10.1152/jappl.1993.74.4.2040.

[21] R. Niedermann, A. Psikuta, R.M. Rossi, Heat flux measurements for use in physiological and clothing research, Int. J. Biometeorol. 58 (2014) 1069–1075, https://doi.org/10.1007/s00484-013-0697-0.

[22] P.J. Rodríguez de Rivera, et al., Advantages of in vivo measurement of human skin thermal conductance using a calorimetric sensor, J. Therm. Anal. Calorim. (2022), https://doi.org/10.1007/s10973-022-11275-x.

[23] P.J. Rodríguez de Rivera, M. Rodríguez de Rivera, F. Socorro, G.M. Callicó, J.A. L. Calbet, M. Rodríguez de Rivera, Heat flow, heat capacity and thermal resistance of localized surfaces of the human body using a new calorimetric sensor, J. Therm. Anal. Calorim. 147 (13) (2022) 7385–7398, https://doi.org/10.1007/s10973-021-11062-0.

[24] P.J. Rodriguez de Rivera, Mi. Rodriguez de Rivera, F. Socorro, M. Rodriguez de Rivera, Calibration and operation improvements of a calorimetric sensor for medical applications, Measurement 186 (2021) 110–134, https://doi.org/10.1016/j.measurement.2021.110134.

[25] P.J. Rodríguez de Rivera, M. Rodríguez de Rivera, F. Socorro, M. Rodríguez de Rivera, Method for transient heat flux determination in human body surface using a direct calorimetry sensor, Measurement 139 (2019) 1–9, https://doi.org/10.1016/j.measurement.2019.02.063.

[26] F. Socorro, M. Rodríguez de Rivera, C. Jesús, A thermal model of a flow calorimeter, J. Therm. Anal. Calorim. 64 (2001) 357–366, https://doi.org/10.1023/A:1011582306796.

[27] R. Kirchner, M.R. de Rivera, J. Seidel, V. Torra, Identification of micro-scale calorimetric devices. Part VI. An approach by RC-representative model to improvements in TAM microcalorimeters, J. Therm. Anal. Calorim. 82 (1) (2005) 179–184, https://doi.org/10.1007/s10973-005-0861-9.

[28] A. Isalgúe, J. Ortin, V. Torra, J. Vīnals, Heat flux calorimeters: dynamical model by localized time constants, Anales de Física, 76 (1980) 192-196.

[29] P.J. Rodríguez de Rivera, M. Rodríguez de Rivera, F. Socorro, M. Rodríguez de Rivera, G.M. Callicó, A method to determine human skin heat capacity using a non invasive calorimetric sensor, Sensors 20 (2020) 3431, https://doi.org/10.3390/s20123431.

[30] J.A. Nelder, C. Mead, A simplex method for function minimization, Comput. J. 7 (1965) 308–313, https://doi.org/10.1093/comjnl/7.4.308.

[31] R. Niedermann, E. Wyss, S. Annaheim, A. Psikuta, S. Davey, R.M. Rossi, Prediction of human core body temperature using non-invasive measurement methods, Int. J. Biometeorol. 58 (1) (2014) 7–15, https://doi.org/10.1007/s00484-013-0687-2.

[32] A.P. Welles, X. Xu, W.R. Santee, D.P. Looney, M.J. Buller, A.W. Potter, R.W. Hoyt, Estimation of core body temperature from skin temperature, heat flux, and heart rate using a Kalman filter, Comput. Biol. Med. 99 (2018) 1–6, https://doi.org/10.1016/j.compbiomed.2018.05.021.

[33] S. Mendt, M.A. Maggioni, M. Nordine, M. Steinach, O. Opatz, D. Belavý, D. Felsenberg, J. Koch, P. Shang, H.-C. Gunga, A. Stahn, Circadian rhythms in bed rest: Monitoring core body temperature via heat-flux approach is superior to skin surface temperature, Chronobiol. Int. 34 (5) (2017) 666–676, https://doi.org/10.1080/07420528.2016.1224241.

[34] S.K. Shenoy, T.E. Diller, Heat flux measurements from a human forearm under natural convection and isothermal jets, Int. J. Heat Mass Transf. 123 (2018) 728–737, https://doi.org/10.1016/j.ijheatmasstransfer.2018.02.068.

[35] R.C. Webb, R.M. Pielak, P. Bastien, J. Ayers, J. Niittynen, J. Kurniawan, M. Manco, A. Lin, N.H. Cho, V. Malyrchuk, G. Balooch, J.A. Rogers, V.M. Ugaz, Thermal Transport Characteristics of Human Skin Measured In Vivo Using Ultrathin Conformal Arrays of Thermal Sensors and Actuators, PloS One. 10 (2) (2015) e0118131, https://doi.org/10.1371/journal.pone.0118131.

[36] https://www.hukseflux.com/products/heat-flux-sensors/heat-flux-sensors. Accesed on 04/05/2022.

[37] Y. Kurazumi, L. Rezgals, A.K. Melikov, Convective heat transfer coefficients of the human body under forced convection from ceiling, J. Ergonomics 4 (2014) 126, https://doi.org/10.4172/2165-7556.1000126.

[38] P.J. Rodríguez de Rivera, M. Rodríguez de Rivera, F. Socorro, M. Rodríguez de Rivera, Measurement of human body surface heat flux using a calorimetric sensor, J. Therm. Biol. 81 (2019) 178–184, https://doi.org/10.1016/j.jtherbio.2019.02.022.